IAC-11.A6.1.14

COMBINATION OF LIGHT CURVE MEASUREMENTS AND ORBIT DETERMINATION FOR SPACE DEBRIS IDENTIFICATION

Carolin Früh
Astronomical Institute, University of Bern, Switzerland
frueh@aiub.unibe.ch

Thomas Schildknecht
Astronomical Institute, University of Bern, Switzerland
thomas.schildknecht@aiub.unibe.ch

Since the first satellite Sputnik was launched 1957, the number of space resident objects has increased constantly. The majority of those objects are so called space debris; objects with no intended use any more. The Astronomical Institute of the University of Bern (AIUB), Switzerland, has maintains a catalogue of space resident objects in geostationary and geostationary transfer orbits for over ten years now. Besides position measurements for orbit determination, also light curve measurements are performed regularly with the Zimmerwald Laser and Astrometry telescope (ZIMLAT), located at Zimmerwald, Switzerland.

The paper investigates the combination of information extracted from optical light curve measurements and information from orbit determination in a comparison of two space debris objects. The analysis focuses on the potential gain for the object characterization, which differs from the known approach to support object identification in the sense, that an orbital element catalogue is combined with light curve measurements, which serve as so called finger prints of objects on an empirical basis.

Orbits are determined with optical observations and these ephemerides can be compared to further observations of the same object, which serve as a ground truth. The residuals, which are found in this comparison, are a measure for the extend to which the parameters estimated in the orbit determination are still a good approximation for the orbit after some time. Light curves are independent of the orbit determination and parameter estimation process, and provide an independent source of information. The main objective of this work is to analyze if the light curves may help understanding the different propagation accuracy of orbits of two similar space debris objects.

I. Introduction

The Astronomical Institute of the University of Bern (AIUB) holds a small catalogue of space debris objects and performs surveys for geostationary (GEO) and geostationary transfer orbits (GTO) since over then years. Some of the objects are also listed in the USSTRATCOM catalogue. Investigated are two decommisioned satellites: 79105A, Gorizont-3, and 80081A, Raduga-7.

Gorizont-3 and Raduga-7 are both Russian communication satellites, which are not

(a) Gorizont

(b) Raduga

Figure 1: Russian communication satellites (a) Gorizont and (b) Raduga [2].

operational anymore. Gorizont satellites have a mass of about 2200 kg and carry eight transponders. They are 3-axis stabilized using liquid propellant micro-engines of the KAUR-3 platform during their life time. The pointing is within 0.5 degrees accuracy towards the Earth's center. The dimensions of the satellites are (including solar panels) 5.45 x 3.30 x 9.46 meters [1]. An image of the satellite model is displayed in Fig. 1a. The Gorizont-3 satellite 79105A is in a geostationary libration orbit around the Eastern stable point with, at present, an inclination of around 14.6 degrees and negligible eccentricity, its estimated AMR value is about 0.007 m^2kg^{-1}.

Raduga satellites have a mass of about 2000 kg and are 3-axis stabilized with the same KAUR-3 platform, which was first deployed in the Raduga satellites and then became a base for the Gorizont models. They have two transponders and their dimensions are (including solar panels) about 5.50 x 2.50 x 9.50 meters [1]. An image of the Raduga satellite model can be found in Fig. 1b. The Raduga-7 satellite 80081A is nowadays in a geostationary libration orbit around the Western stable point with an inclination of about 14.4 degrees and negligible eccentricity, its estimated AMR value is about 0.018 m^2kg^{-1}.

Both objects seem to be very similar and in comparable orbits. In a first step, orbits of both objects are determined with different number of estimated parameters and the propagation accuracy is determined. In a second step different light curves of both objects are compared. All observations and light curves stem from the one meter Zimmerwald Astrometry and Laser Telescope (ZIMLAT).

II. Orbits

Orbits of both objects have been determined with an enhanced version of the CelMech tool [3]. For both objects different orbits have been determined with a short and longer fit interval. CelMech allows to estimate not only the orbital elements, but it can also be chosen to estimate in addition the area-to-mass ratio (AMR) as scaling parameter for the direct radiation pressure (DRP) acceleration. If the AMR is not estimated a default value of 0.02 m^2kg^{-1} is used.

In addition, CelMech allows to estimate so-called empirical, constant once per revolution (DRP-) parameters decomposed in the RSW-directions, whereas the R-direction points from the geocenter to the satellite, S-direction in the along-track direction, orthogonal to the radial direction, in direction of the velocity of the object and the W-direction is orthogonal to the orbital plane and completes the right hand system.
In a first step the orbits are propagated and ephemerides are generated past the fit interval of orbit determination and compared to further observation of the same object. The accuracy of observations of the ZIMLAT telescope are below 0.5 arcseconds, as regular monitoring of the observation accuracy via high precision ephemerides of GNSS satellites, provided by the International GNSS Service (IGS), which is located at the AIUB, shows. The comparison to further observations are therefore a good measure for the propagation accuracy. The ephemerides are compared in angular distance on the celestial sphere and in projected along-track and cross-track direction in the tangent plane, scaled with the radial distance of the ephemerides.
The orbits determined for the two objects, are characterized in Tab. 1. The columns show

Table 2: Characterization of different orbits for the object 80081A.

	OD 1	**OD 2**	**OD 3**	**OD 4**	**OD 5**
start epoch [MJD]	54115.778604	54130.767031	54147.892958	54152.176868	54171.042372
end epoch [MJD]	54145.034616	54152.176868	54170.141564	54174.158928	54196.909040
time interval [d]	30	22	23	22	25
number of obs.	32	17	13	18	20
rms [$\ddot{}$]	0.26	0.29	0.87	0.23	0.52
osc. elements at	54171.042372				
a [m]	42172565.001	42172568.762	42172522.508	42172466.451	42172517.235
	±0.127	±4.843	±9.211	±13.269	±2.804
e	0.0003366	0.0003482	0.0003527	0.0003463	0.0003482
	±0.0000005	±0.0000028	±0.0000027	±0.0000038	±0.0000013
i [deg]	14.360502	14.360504	14.360487	14.360607	14.360451
	±0.000020	±0.000005	±0.000104	±0.000044	±0.000075
RA of node [deg]	1.392344	1.392743	1.392228	1.392291	1.392585
	±0.000060	±0.000016	±0.000325	±0.000069	±0.000167
AMR [m^2kg^{-1}]	0.014751	0.015542	0.022678	0.006224	0.014786
	±0.000096	±0.000085	±0.003698	±0.003820	±0.000803

Table 1: Characterization of orbits for the GEO objects 79105A, 80081A. Time interval in days, number of observations, root mean square of orbit determination in arcseconds, AMR in m^2kg^{-1}, rms of orbit determination in m^2kg^{-1}.

	time	# Obs	rms	AMR	rms (AMR)
79105A					
$EPHM_S$	10	18	0.61	0.02000	-
$EPHM_L$	32	23	1.11	0.02000	-
$EPHM_{LDRP}$	32	23	0.48	0.00691	$\pm 8.93 \cdot 10^{-3}$
80081A					
$EPHM_S$	5	11	0.20	0.02000	-
$EPHM_M$	15	25	0.28	0.02000	-
$EPHM_{MDRP}$	15	25	0.21	0.01255	$\pm 1.19 \cdot 10^{-3}$
$EPHM_L$	29	32	1.72	0.02000	-
$EPHM_{LDRP}$	29	32	0.26	0.01475	$\pm 9.61 \cdot 10^{-5}$

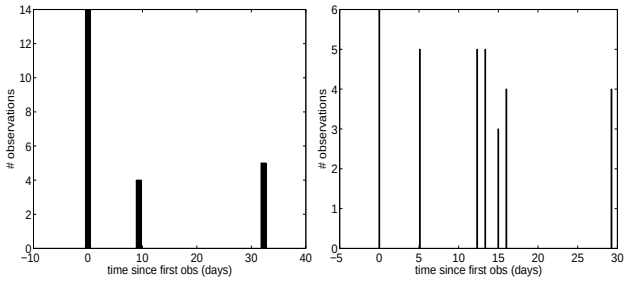

(a) 79105A (b) 80081A

Figure 2: Time distribution of the observations used in orbit determination for the GEO objects (a) 79105A, (b) 80081A.

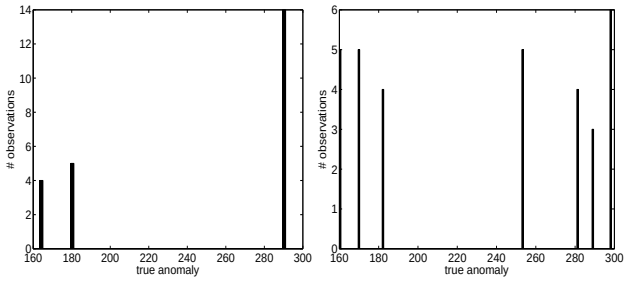

(a) 79105A (b) 80081A

Figure 3: Anomaly distribution of the observations used in orbit determination for the GEO objects (a) 79105A, (b) 80081A.

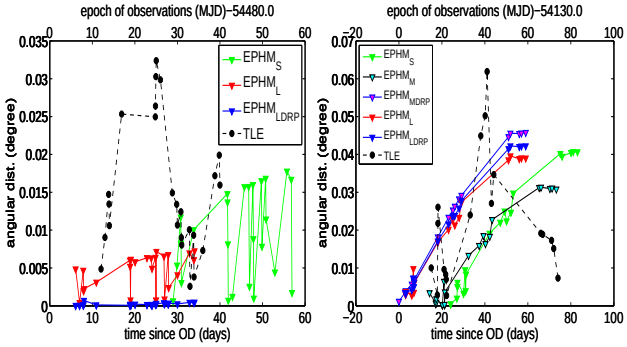

(a) 79105A (b) 80081A

Figure 4: Angular distances in degrees between the observations and predicted ephemerides using either TLE data or determined orbits for the GEO objects (a) 79105A, (b) 80081A as a function of epoch of the observations for TLE data and the time since orbit determination for the orbits.

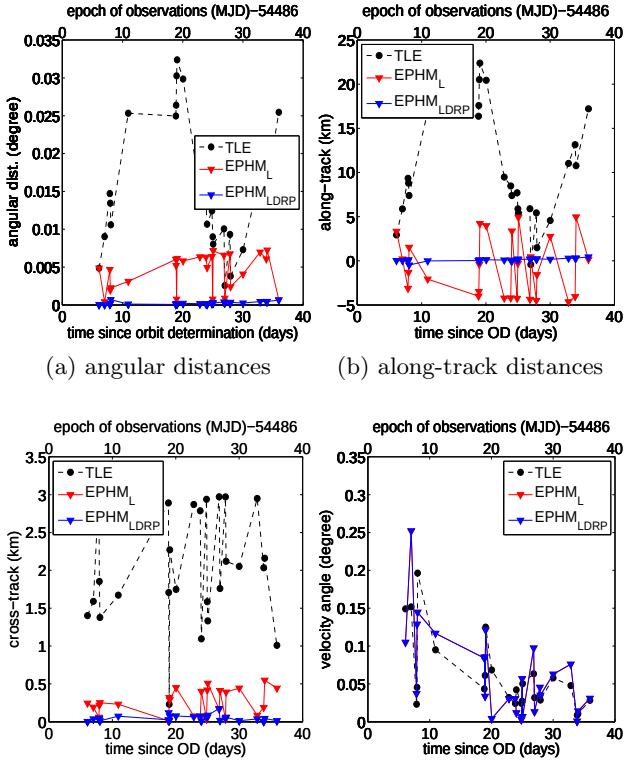

(a) angular distances (b) along-track distances

(c) cross-track distances (d) angle between velocity directions

Figure 5: Distances between observed positions and predicted ephemerides from TLEs and from orbit determinations and predictions with CelMech for GEO object 79105A as a function of epoch of the observations for TLE data and the time since orbit determination for the orbits.

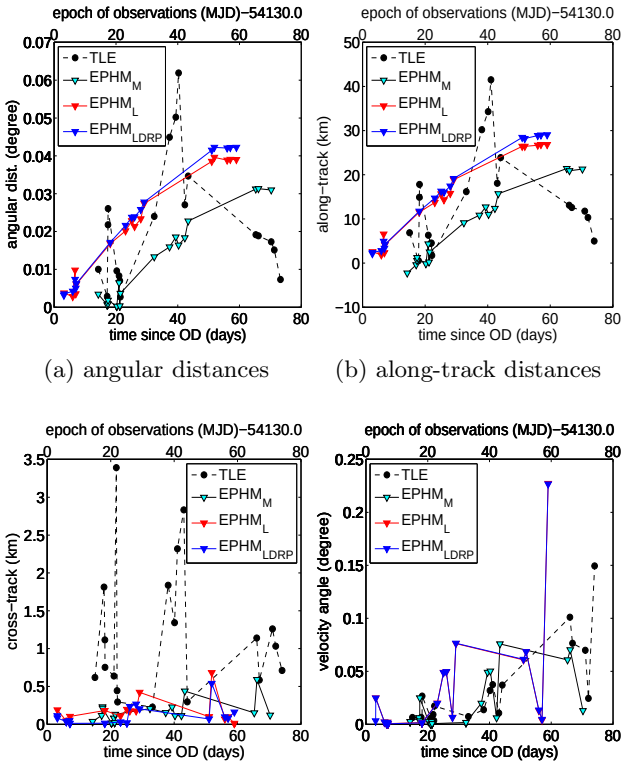

(a) angular distances (b) along-track distances

(c) cross-track distances (d) angle between velocity directions

Figure 6: Distances between observed positions and predicted ephemerides from TLEs and from orbit determination for GEO object 80081A as a function of epoch of the observations for TLE data and the time since orbit determination for the orbits.

the length of the interval fit interval of orbit determination covered by observations, the number of observations within this fit interval, the root mean square (RMS) error of the orbit determination, the AMR value and its rms error. If the AMR value is not estimated, self-evidently no error for the AMR value is given.

Figure 2 shows the distribution of observations, which were used in the orbit determination, for both objects. The corresponding true anomalies are shown in Fig. 3.

Figure 4 shows the angular distances between the observed astrometric positions and the astrometric positions calculated from the ephemerides of the determined and predicted orbits as a function of time since the last epoch within the fit interval of the orbit determination. The additional observations were *not* used for orbit determination. In addition, the angular distances between the observed astrometric positions and TLE ephemerides of the USSTRATCOM catalogue are shown as a function of the epoch of the astrometric positions. The TLE ephemerides were calculated with different TLE sets, each closest to the particular observation epoch. For the accuracy of TLE ephemerides in GEO please refer to [4]. The displayed values are averages of each observation/ephemerides tracklet. A tracklet consists of three to six single data points, spaced by 30 seconds.

Figure 4a shows that the orbit $EPHM_S$ of object 79105A, determined over an fit interval of ten days, produces large angular distances in the prediction. The ephemerides of orbits over a larger fit interval of 32 days, $EPHM_L$ and $EPHM_{LDRP}$, show smaller distances to the observations. As Fig 5 shows, the ephemerides orbit $EPHM_L$, for which no AMR value was estimated show large variations, mainly in along-track but also in cross-track direction. The ephemerides of $EPHM_{LDRP}$ with an estimated AMR value of about 0.069 $\mathrm{m^2kg^{-1}}$ show the smallest residuals, of below 0.002 degrees. The angles between the velocity directions are very similar for the ephemerides of the different orbits and ephemerides of TLE data. With an observation accuracy of the order of about 0.5 arcseconds, errors in the velocity angle of below $6.4 \cdot 10^{-2}$ degrees may just reflect the observation errors.

For object 80081A, the distances between the observations and the computed ephemerides show a secular trend, all distances are increasing rapidly as a function of prediction time, see Fig. 4. The distances of the observations to the TLE ephemerides are smaller than to the ephemerides of the determined orbits, despite the fact that the distances of the TLE ephemerides are of the same order of magnitude as for the other object. Figure 6 shows particularly in along-track a large secular trend. The differences rise fast with the prediction time, the differences in cross-track direction are small and do not show a significant trend. This is the case for the orbit determined over 15 days ($EPHM_M$) or over 32 days with ($EPHM_{LDRP}$) or without ($EPHM_L$) estimating an AMR value. The smallest distances are associated with the orbit $EPHM_M$ and not with the orbit $EPHM_L$, which was determined over a longer fit interval. As opposed to the objects 79105A the smallest differences are not achieved with orbits including the estimation of an AMR value, all differences are in general larger than for object 79105A. The observations used for orbit determination are well distributed in time and anomaly, see Fig. 2b and 3b.

Further orbits were determined with the subsequent overlapping fit intervals. The results are listed in Tab. 2. OD 2 could only be determined when estimating an empirical R-parameter in addition to the DRP value. The osculating orbital elements at the reference epoch of all determined orbits do not differ significantly. The orbital elements show the largest errors for OD 3 and OD 4. Those orbits also show significantly different AMR values, compared to the other orbits. But the error in the AMR value

Table 3: Characterization of two different orbits for the object 80081A..

	OD 125	**OD 34**
start epoch $[MJD]$	54115.778604	54147.892958
end epoch $[MJD]$	54196.909040	54174.158928
number of obs.	69	31
rms $[\ddot{]}$	0.84	0.73
osc. elements at	54196.909	
a [m]	42172569.080	42172506.673
	$\pm$0.613	$\pm$2.036
e	0.0003642	0.0003504
	$\pm$0.0000011	$\pm$0.0000010
i [deg]	14.360498	14.360525
	$\pm$0.000121	$\pm$0.000052
RA of node $[deg]$	1.392668	1.392338
	$\pm$0.000307	$\pm$0.000127
AMR $[\mathrm{m^2kg^{-1}}]$	0.007530	0.017921
	$\pm$0.000363	$\pm$0.000106

is also larger than that of the other orbits. It is not possible to determine a low rms orbit over all observations of OD 1 to OD 5, from epoch 54115.8 to 54171.0: Even when estimating additional empirical parameters no orbit could be determined with an rms value of below 10 arcseconds. An orbit can be determined with the observations of the fit intervals of OD 1, OD 2, and OD 5, named OD 125 in the following, when the AMR as well as empirical R- and W-parameters were estimated. A small rms orbit resulted as well when determined with observations of the fit intervals of OD 3 and OD 4. The osculating orbital elements, AMR value, their errors and the rms are listed in Tab. 3. The osculating orbital elements do show small differences at the reference epochs. But a significantly different AMR value has been determined. Between epoch 54147.9 and 54152.1 a property of the object may have changed. The change may cause the differences in the estimated AMR values.

Table 4: Light curve measurements for object Gorizont-3 79105A: Date, start epoch in modified Julian Date, phase angles in degrees.

Date	epoch	ϕ	ϕ_{xy}	ϕ_{xz}
Feb 2 2008	54499.0	40.5 to 54.0	35.4 to 48.9	26.6 to 30.2
Feb 3 2008	54499.8	16.6 to 11.7	13.8 to 2.9	9.7 to 14.7
Feb 7 2008	54503.9	16.8 to 20.7	9.7 to 14.6	17.6 to 18.9
Feb 18 2008	54514.8	26.7 to 10.7	26.6 to 6.0	1.82 to 9.9
Aug 8 2010	55417.1	80.5 to 85.3	78.8 to 83.3	26.1 to 27.7
Sep 21 2010	55461.0	56.7 to 61.6	56.3 to 61.3	13.1 to 16.0
Dec 9 2010	55539.8	18.3 to 15.3	11.1 to 6.1	41.6 to 36.5
Dec 26 2010	55557.0	30.0 to 50.8	25.4 to 47.4	66.3 to 75.9
Jan 2 2011	55564.0	52.0 to 55.4	47.8 to 51.2	62.3 to 63.2

III. Light Curves

For both objects, 79105A and 80081A, light curve measurements have been taken. A selection of the light curves measured of 79105A are displayed in Fig. 7. The displayed light curves were taken in 2008 on January 18, in 2010 on August 8, September 21, December 9, December 26, and in 2011 on January 2. The different phase angles are determined: The phase angle ϕ is the classical phase angle, observer – sun – object. In addition, a coordinate system in the center of mass of the object is determined, with a fundamental plane (xy-plane) parallel to the earth equator, the x-direction is aligned with the topocentric earth fixed direction to Greenwich, the z-direction completes the right hand system. This allows to determine the projection of the phase angle ϕ, in the xy-plane, ϕ_{xy}, and in the xz-plane, ϕ_{xz}.

The dates, start times and the variation of the different phase angles – $\phi/\phi_{\mathrm{xy}}/\phi_{\mathrm{xz}}$ – during the measurement are listed in Tab. 4. Brightness variations of more than two magnitudes are measured. In the light curve displayed in Fig. 7(f) even variations of over five magnitudes do occur. This light curve was observed under an overall phase angle and phase angle $\phi/\phi_{\mathrm{xy}}/\phi_{\mathrm{xz}} \approx 60/60/14$ degrees. There seem to be displayed a similar but not

Table 5: Light curve measurements for object Raduga-7 80081A. Date, start epoch in modified Julian Date, phase angles in degrees.

Date	epoch	ϕ	ϕ_{xy}	ϕ_{xz}
Sep 21 2010	55461.1	20.9 to 23.9	20.8 to 23.7	2.3 to 3.1
Oct 5 2010	55475.0	23.7 to 21.2	21.1 to 15.6	11.1 to 10.4
Dec 9 2010	55539.8	99.4 to 94.7	96.6 to 91.9	70.1 to 68.6
Dec 13 2010	55544.0	38.9 to 34.4	36.7 to 31.8	60.6 to 58.8
Dec 26 2010	55556.9	63.3 to 41.8	62.9 to 40.6	96.6 to 88.6
Jan 2 2011	55563.9	54.0 to 49.3	53.9 to 49.0	107.0 to 104.9

identical brightness variation pattern in all light curves, although the light curves were observed under different phase angles. No clear dependency on the brightness or the peculiarity of the pattern on the different phase angles can be determined.

Six light curves of the object Raduga-7, 80081A, are displayed in Fig. 8. They have been taken on six different nights from September 2010 to January 2011. The dates, and the variation of the phase angles, ϕ, ϕ_{xy} and ϕ_{xz} are displayed in Tab. 5.

There is a similar brightness pattern visible in all light curves, but the time distribution of the pattern varies heavily. The pattern seems to be spread over far longer time intervals in Fig. 8(a) and Fig. 8(b). Those are the light curves taken under the smallest phase angle in the selection of light curves displayed in Fig. 8. The 79105A satellite does not show such a phase angle dependency.

IV. Conclusions

The orbits and light curves of two similar decommissioned Russian communication satel-

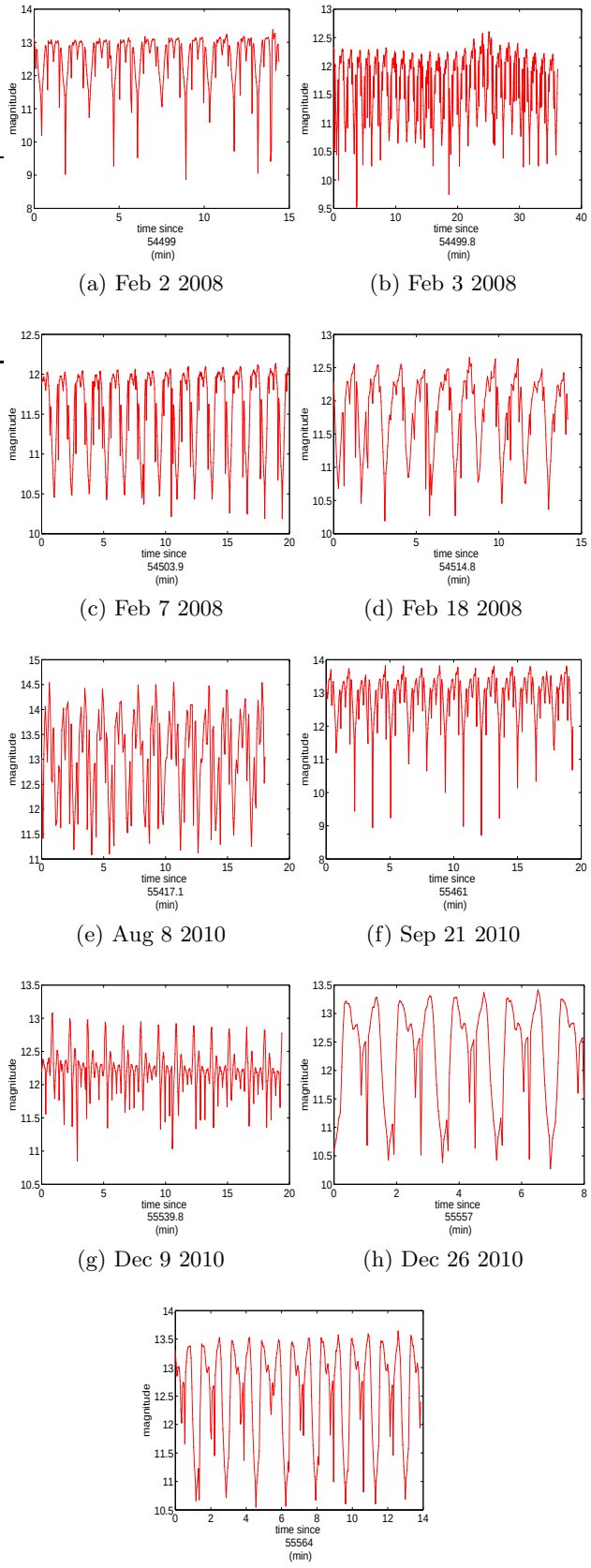

(a) Feb 2 2008 (b) Feb 3 2008

(c) Feb 7 2008 (d) Feb 18 2008

(e) Aug 8 2010 (f) Sep 21 2010

(g) Dec 9 2010 (h) Dec 26 2010

(i) Jan 2 2011

Figure 7: Light curves measurements of the object of Gorizont-3 79105A over time: (a) Feb 2 2008, (b) Feb 3 2008, (c)Feb 7 2008, (d) Feb 18 2008, (f) Sep 21 2010, (g) Dec 9 2010, (h) Dec 26 2010, (i) Jan 2 2011.

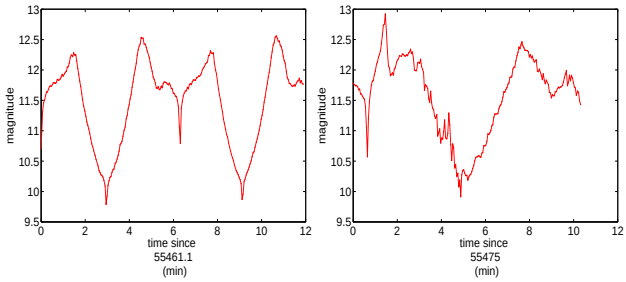

(a) Sep 21 2010

(b) Oct 5 2010

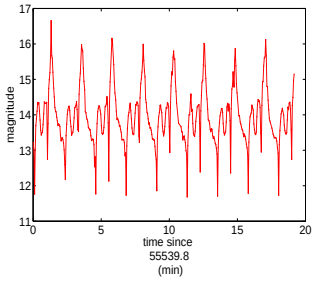

(c) Dec 9 2010

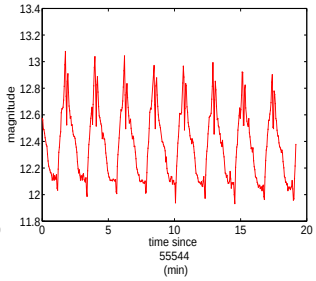

(d) Dec 13 2010

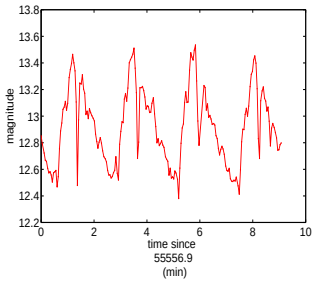

(e) Dec 26 2010

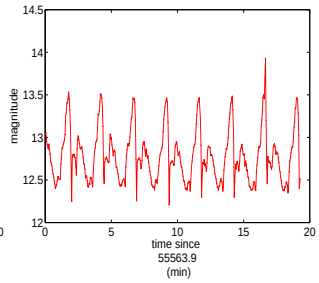

(f) Jan 2 2011

Figure 8: Light curves measurements of the object Raduga-7 80081A over time: (a) Sep 21 2010, (b) Oct 5 2010, (c) Dec 9 2010, (d) Dec 13 2010, (e) Dec 26 2010, (f) Jan 2 2011.

lites, Gorizont-3, 79105A, and Raduga-7, 80081A, with low area-to-mass ratio (AMR) have been investigated. They both have been in the same stabilization mode but are now decommissioned and not actively stabilized any more. The objects are in comparable geostationary drift orbits.

The orbits determined over different fit intervals and with different number of estimated parameters revealed that the propagated ephemerides of the orbits of object 79105A show small distances to further observations, whereas all orbits of the object 80081A a show large secular trend. Further orbit determination with overlapping fit intervals of the latter object suggested, that the AMR does not seem to be stable over time. The light curves are supporting the assumption that object 80081A may not be in a stable attitude state, in contrary to object 79105A. The light curves also clearly show, that a fingerprinting, which is stable over longer time intervals, is even for such a large space debris objects with low area-to-mass ratio not always possible, even the pattern of the more stable object 79105A is subject to change over time.

V. Acknowledgments

Many thanks go to Martin Ploner, the technical head of the Zimmerwald Observatory, responsible for the operational software to take light curves with such a good sampling rate and to our observers, who supported me in gaining light curves: Marcel Prohaska, Johannes Herzog, Alexander Scartazzini, Stefan Funariu, Alexander Läderach, Simon Willi, Sarah Arnolds.

The work was supported by the Swiss National Science Foundation through grants 200020-109527 and 200020-122070.

References

[1] Russian Space Web Homepage. by Anatoly Zak. `http://www.russianspaceweb.com/`, 2011.

[2] Sykrocket Homepage. by Gunter Krebs. `http://www.skyrocket.de/`, 2011.

[3] G. Beutler. *Methods of Celestial Mechanics*. Two Volumes. Springer-Verlag, Heidelberg, 2005. ISBN: 3-540-40749-9 and 3-540-40750-1.

[4] C. Früh, T. Schildknecht, R. Musci, and M. Ploner. Catalogue Correlation of Space Debris Objects. In *Proceedings of the Fifth European Conference on Space Debris, ESOC, Darmstadt, Germany, 30 March-2 April 2009*, 2009.